Superlattices and Microstructures 130 (2019) 28–37

Contents lists available at ScienceDirect

Superlattices and Microstructures

journal homepage: www.elsevier.com/locate/superlattices

Study of deep level defects in InGaP/InGaAs-GaAsP/InGaAsN quantum well based multi-junction solar cell using finite element analysis

M. Sukeerthi[a], Siva Kotamraju[a,*], Suresh E. Puthanveettil[b]

[a] IIIT Chittoor, Sri City, Andhra Pradesh 517646, India
[b] U. R. Rao Satellite Centre, Bengaluru 560017, India

ARTICLE INFO

Keywords:
III-V MQW solar cells
Dilute nitrides
Carrier removal
Deep level traps
Effective carrier lifetime
Device modeling

ABSTRACT

Degradation analysis of a quantum well-dilute nitride based multi-junction solar cell is presented using a 2D numerical device simulator: APSYS. By taking carrier removal effects into consideration, the proposed device exhibits strong electric field uniformity within the intrinsic region of the p-i-n middle cell. The electron traps are defined in the top InGaP and bottom InGaAsN base region considering 1 MeV electron irradiation in geostationary orbits. Considering thermionic emission, tunneling and SRH lifetime an effective lifetime value of 16.7 ps is considered in the middle MQW region. A record efficiency value of 38% and 44% is obtained at 1-sun and 500-sun AM0 spectrum respectively. The same efficiency value dropped by 4% by introducing a realistic SRV (1×10^4 cm s^{-1}) and trap concentration values (1×10^{16} cm^{-3}). Finally, we illustrate the influence of traps and lifetime on overall cell J_{sc}, V_{oc}, η, and power density.

1. Introduction

Multi-junction solar cell (MJSC) based on InGaP/GaAs/Ge is commercialized and are currently being used for powering space satellites [1,2]. Compared to single junction or single band gap, multi-junction helps in minimizing thermalization losses by effectively splitting the spectrum (from 230 nm to 1800 nm) between the cells [3]. However, the efficiency of the existing device is limited to 31% at 1-sun AM0 spectrum [4]. To bypass the Shockley-Queisser limit and to improve efficiency further among third generation solar cells, quantum well and quantum dot solar cells are currently being explored [5,6]. Conventional p-n diode of middle cell was replaced by p-i-n structure, with alternate well and barrier layers being employed within the intrinsic (i)- region [7,8]. The multiple quantum well (MQW) incorporated solar cells have an added advantage of tuning the QW bandgap to match the incident photon energy. In this paper, $In_{0.10}Ga_{0.90}As$ quantum wells with a band gap less than that of GaAs host material were introduced within the i-region. The MQW stack that encounters low energy photons produce excess minority carriers and therefore contributes to higher photocurrent [9]. Introducing dilute nitride based quaternary alloy InGaAsN below GaAs subcell has been explored earlier as one of the promising ways to improve the efficiency. This is because InGaAsN has excellent lattice matching with GaAs and has a band gap (~1.1 eV) lower than GaAs [10]. Although, addition of 2% nitrogen to GaAs lowers the band gap to ~1.1 eV, it also introduces electron trap at Ec-0.2 eV severely affecting the diffusion length of minority carriers. Annealing of the sample has shown improvement in photovoltaic properties earlier [11]. In spite of certain difficulties with dilute nitride layer, world record efficiencies have been demonstrated by incorporating in MJSC [12–14]. Although, there has been papers published exploring dilute nitrides and

* Corresponding author.
E-mail addresses: sukeerthi.m@iiits.in (M. Sukeerthi), siva.k@iiits.in (S. Kotamraju), eps@isac.gov.in (S.E. Puthanveettil).

https://doi.org/10.1016/j.spmi.2019.04.009
Received 3 March 2019; Accepted 3 April 2019
Available online 10 April 2019
0749-6036/

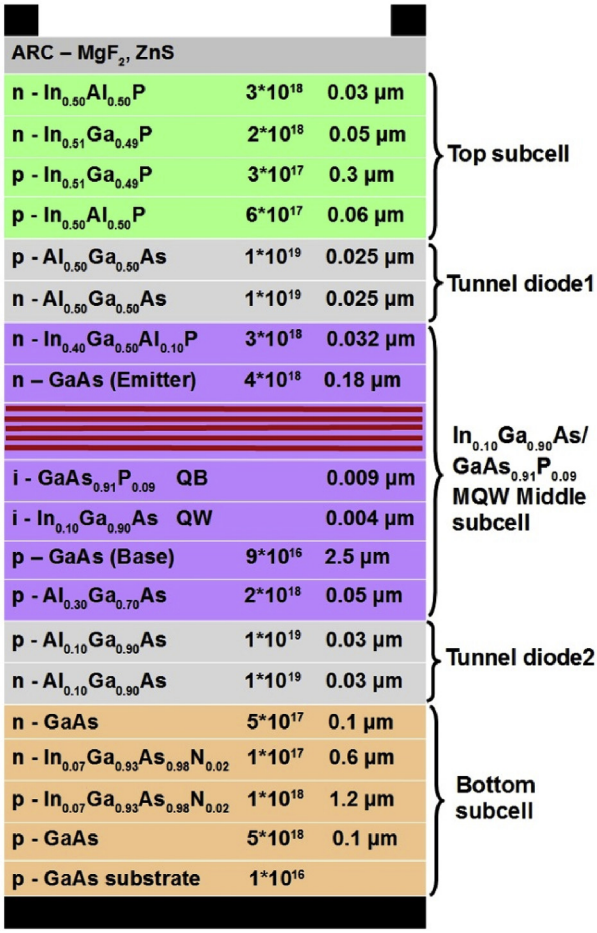

Fig. 1. Schematic illustration of 3J InGaP/InGaAs QW-GaAsP QB/InGaAsN solar cell (doping values in cm^{-3}).

quantum wells separately, there has been no work published till date combining these two concepts. Among InGaP, GaAs and Ge subcells, GaAs was found to be the current limiting subcell after subjecting to irradiation [15,16]. In this paper, we replace current limiting GaAs middle subcell with GaAsP quantum barrier (QB)-InGaAs quantum well (QW) based on reference [17] and include InGaAsN as the third subcell instead of Ge [18,19]. The triple junction (3J) InGaP/(InGaAs-GaAsP)/InGaAsN solar cell structure was designed and simulated with the help of software simulation tool Crosslight APSYS [20]. The numerical simulator solves Poisson's equation and drift/diffusion equations to model the device characteristics. Conventional 3J InGaP/InGaAs/Ge solar cell modeling using APSYS was reported earlier in Refs. [21–23]. We first simulated the conventional 3J solar cell and ensured it is closely matching with the experimental J-V of a commercial solar cell before making changes to the device structure. MgF_2 and ZnS anti-reflective coatings were used on top of the solar cell to increase the photon absorption [24,25]. The top, middle, and bottom subcells are connected in series by highly doped AlGaAs tunnel junctions [26].

2. Comparison of 3J MQW and 3J p-i-n solar cell characteristics

Two triple-junction solar cells with middle p-i-n structure for one cell and middle MQW structure for the other cell were simulated. 3J InGaP/InGaAs QW-GaAsP QB/InGaAsN solar cell structure is shown in Fig. 1. Fig. 2 presents J-V characteristics and Table 1 compares the output parameters of the two solar cells. The efficiency of 3J MQW solar cell is high compared to the one without MQW by almost 4%. Including multiple quantum wells in the middle subcell extends the absorption edge [27] that enhances V_{oc} [28], J_{sc} and efficiency [9] compared to the solar cell without quantum wells. The QW and QB thickness values were strain-balanced [29,30] to attain higher efficiency. In our simulations, the QW and QB were 4 and 9 nm thick respectively, with five wells and barriers inserted in middle cell intrinsic region. Surface states formed due to abrupt interruption of semiconductor lattice act as recombination centers. The minority electrons/holes which encounter these states recombine, which affects the carrier flow, thus decreasing the solar cell efficiency. Modeling the MJSC with a realistic 1×10^4 cm s^{-1} electron/hole surface recombination velocity (SRV) defined at the window-emitter interface and base-back surface field (BSF) interface of each subcell, estimates the drop experienced by the solar cell parameters due to surface states. Restricting the SRV to a value equal to or less than 1×10^4 cm s^{-1} is important beyond

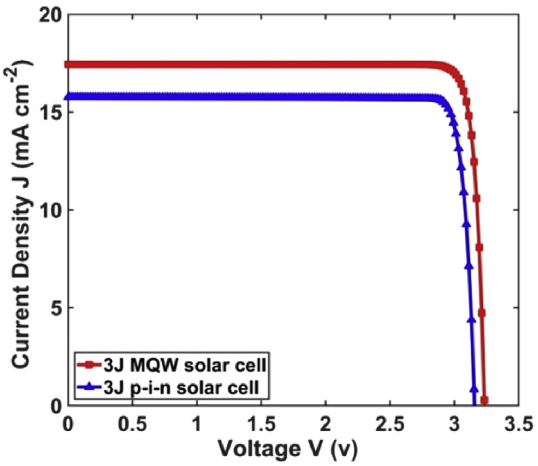

Fig. 2. Current density (J)-voltage (V) characteristics of MJSC with middle MQW structure for one cell and middle p-i-n structure for the other.

Table 1
Output parameters of 3J MQW and 3J p-i-n solar cells.

	MJSC(MQW middle cell)	MJSC(p-i-n middle cell)
J_{sc} (mA/cm^2)	17.436	15.76
V_{oc} (v)	3.233	3.156
Efficiency η (%)	37.91	33.59

which the cell experiences more degradation [21]. The 3J InGaP/$In_{0.10}Ga_{0.90}As$ QW-$GaAs_{0.91}P_{0.09}$ QB/InGaAsN solar cell produced an efficiency of 38.14% and 37.91% without SRV and at an SRV of 1×10^4 cm s^{-1} respectively. Further simulations were given by fixing an SRV of 1×10^4 cm s^{-1} at window-emitter and base-BSF interfaces of all subcells.

3. Results

This section is divided into three subsections. The electric field variation within the MQW region by assuming carrier removal (CR) effect is studied in Section 3.1. Section 3.2 focused on the device characteristics by plotting total cell J_{sc}, V_{oc}, and η variation with respect to trap concentration of deep level traps. The last section includes analysis of the total cell power density variation with applied bias voltage, brief discussion on efficiency vs. sun concentration plot and EQE curves.

3.1. Electric field vs. depth within MQW region

A heavy dose of space irradiation results in crystal defects within a material that varies the material doping profile, predominantly affecting the cell performance. This phenomenon is termed as CR effect [31]. Due to the occurrence of CR, the intrinsic material doping changes to either n- or p-type. We presented results for n-type conversion of i-region, since it has been reported for group III-V materials [32]. Maintaining a constant or uniform electric field across MQW intrinsic region is important in determining the carrier movement within that region. This uniformity of the field deviates when the device undergoes CR effect. To incorporate the CR effect within the middle cell, the intrinsic region is changed to n-type doped region. Simulations were carried out to study the MQW region electric field variation under CR effect. The electric field also depends on bias voltage. The magnitude of electric field is reduced by applying bias voltage. Fig. 3a illustrates the electric field variation across InGaAs-GaAsP region at $V_{bias} = 3.5$ volts, with the intrinsic region changed to n-type. At emitter-QW and QW-base interfaces, it can be noticed that electric field magnitude is high. This is the region where potential experiences steep rise depleting the carriers in the emitter and base regions that are close to i-region [33]. As can be seen, the electric field value is 80 kV/cm when the MQW region remains intrinsic. The slope of the field line can be approximated to zero. The electric field profile becomes non-uniform as the intrinsic region doping changes to n-type material (5×10^{16} cm^{-3}). Here, the slope of the electric field attains a non-zero value and affects the carrier transport within the quantum well region thereby reducing the device current. It can be noticed from the Fig. 3a that the field drops more in the emitter region compared to the base region as the i-region doping turns n-type. This point can be strengthened by the following discussion: a) The electron-hole pairs generated, within the i-region and within the diffusion length of electrons and holes in both p and n-regions, are separated by the drift electric field present across the depletion region of p-i-n structure. The built-in-potential V_{bi} of the GaAs p-i-n diode considered in this paper is 1.379 volts. V_{bi} for p-i-n junction is given by

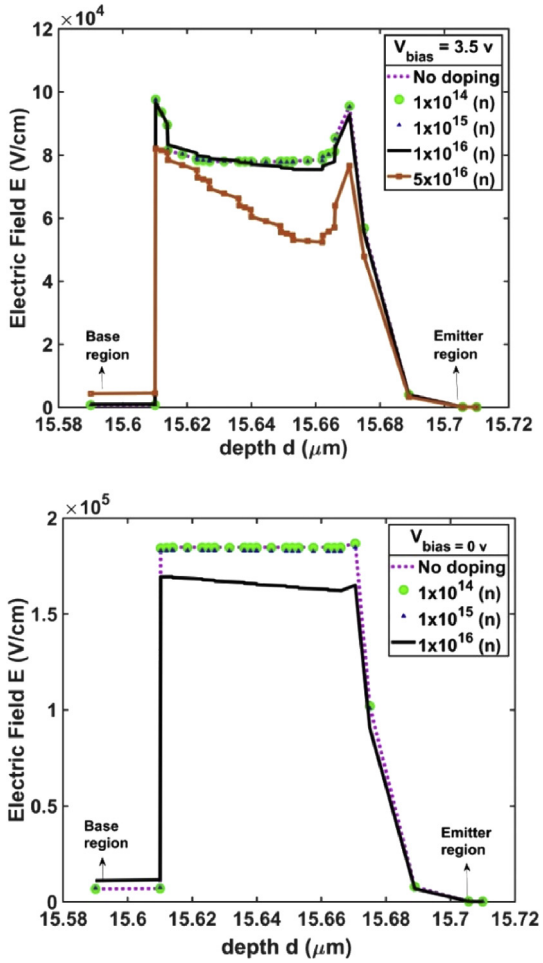

Fig. 3. Electric field E variation across MQW region with varying carrier concentration of i-region at two bias voltages (a) V_{bias} = 3.5 volts (b) V_{bias} = 0 volts. The CR effects were analysed by changing the MQW region background doping from intrinsic to n-type ($1 \times 10^{14}\,cm^{-3}$ - $5 \times 10^{16}\,cm^{-3}$).

$$V_{bi} = \frac{kT}{q} \ln\left(\frac{N_a{}^* N_d}{n_i^2}\right) \tag{1}$$

b) When the i-region changes to n-type due to CR effect, p-n-n + structure is formed, reducing the V_{bi} at both p-n and n-n + junctions. The V_{bi} values for both p-n and n-n + junctions are 1.26 and 0.114 volts respectively. V_{bi} for n-n + region is given by [34]

$$V_{bi} = \frac{kT}{q} \ln\left(\frac{N_d^+}{N_d}\right) \tag{2}$$

The built-in-potential dropped to a very less value at emitter region compared to the base region. The electric field and the built-in potential are related by the following equation.

$$\frac{dV_{bi}}{dx} = -E(x) \tag{3}$$

Hence, the electric field has reduced more closer to the emitter region compared to the base region. This means the generated carriers at QW-base interface can be separated easily due to high amplitude field value compared to the one generated at QW-emitter interface. At this interface, the minority carriers are not subjected to constant electric field within the MQW region and cannot reach the other end for current conduction. They may recombine and reduce the overall cell performance. It is recommended that the i-region doping should be preferably below $1 \times 10^{15}\,cm^{-3}$ to maintain uniform electric field sufficient to collect carriers generated in the MQW region [9]. The simulations were repeated to produce electric field vs. depth plot without applying any bias voltage. Fig. 3b presents the MQW region electric field variation with intrinsic region being changed to n-type doping. The field remained almost constant when the doping is in a transition from intrinsic to $1 \times 10^{15}\,cm^{-3}$ (n-type) material. The field value slightly deviates when the intrinsic carrier concentration changes to $1 \times 10^{16}\,cm^{-3}$. This deviated field affects the charge carrier movement within the

Table 2
Material parameters of QW-$In_{0.10}Ga_{0.90}As$, QB-$GaAs_{0.91}P_{0.09}$ and $In_{0.49}Ga_{0.51}P$.

Parameters (Symbol, Units)	Band-gap (E_g, eV)	Effective mass (m_n)
QW-$In_{0.10}Ga_{0.90}As$	1.264	0.0255 [29]
QB-$GaAs_{0.91}P_{0.09}$	1.52	0.0263 [29]
$In_{0.49}Ga_{0.51}P$	1.86	0.11 [36]

MQW region. Further simulations were given by fixing $1 \times 10^{16}\,cm^{-3}$ n-doping within MQW region [35] at $V_{bias} = 3.5$ volts.

3.2. Degradation of solar cell output parameters

The solar cells in the space environment are usually subjected to high energetic particles such as electrons and protons that induce traps within the cell layers affecting its overall performance. Considering particles of one type, a reasonable assessment of solar cell degradation can be made [39]. To simulate the irradiated device behaviour, we considered deep level traps due to electron irradiation to be present in thick base regions of top and bottom cells. For this, the simulation models presenting minority electron diffusion length dependence on trap concentration were used for top InGaP and bottom InGaAsN materials [21,40]. The trap concentration values and their corresponding minority electron lifetimes were defined in the base regions of top and bottom cells. The lifetime of charge carriers across the MQW region plays a crucial role in deciding the carrier movement and their collection, which contributes to the photocurrent. The carrier movement in quantum wells is governed by thermionic and tunneling mechanisms [41]. An effective lifetime τ_{eff} is fixed for the quantum well region and it is calculated by considering thermionic emission lifetime τ_E, tunneling lifetime τ_T and non-radiative recombination lifetime τ_R. τ_{eff}, τ_E, τ_T, and τ_R are related by [42].

$$\frac{1}{\tau_{eff}} = \frac{1}{\tau_E} + \frac{1}{\tau_T} + \frac{1}{\tau_R} \tag{4}$$

We assumed that non-radiative recombination is the major recombination mechanism neglecting the effect of radiative recombination. τ_T and τ_R were fixed at 130 ps [43] and 10 ns [35] respectively. Based on the material parameters listed in Table 2, the thermionic emission lifetime was calculated to be 19.25 ps. An effective carrier lifetime of 16.74 ps was defined in the MQW region while giving simulations. By introducing deep level traps, we analysed the degradation of solar cell output parameters. These traps are defined by specifying the trap concentration, trap type, energy level, and capture cross section values for InGaP and InGaAsN materials as specified in Table 3. Fig. 4a–c depict the variation of J_{sc}, V_{oc}, and efficiency (η) with respect to trap concentration. Initially, J_{sc} remains constant and starts reducing beyond a trap concentration of $1 \times 10^{16}\,cm^{-3}$. The degradation onset in case of V_{oc}, got initiated at $1 \times 10^{15}\,cm^{-3}$ trap concentration. At a trap concentration higher than $1 \times 10^{16}\,cm^{-3}$, this drop can be ascribed to the fact that diffusion length falling below the *p*-InGaP and p- InGaAsN base regions thickness. It is to be noted that the percentage drop of degradation in case of V_{oc} is high compared to the drop in J_{sc}. Reduction of minority carrier diffusion length reduces the number of photo generated carriers that pass the depletion region. This lowers the carrier collection and hence J_{sc}. Simultaneously, the reverse dark saturation current J_{01} increases due to decrease in diffusion length of minority carriers. J_{01} and diffusion length L_n are related by [44]

$$J_{o1} = \frac{q n_i^2}{N_A} \frac{D_n}{L_n} \tag{5}$$

V_{oc} value decreases with increase in J_{01} as it is logarithmically proportional to inverse of J_{01}

$$V_{oc} = \frac{kT}{q} \ln \frac{J_{sc}}{J_{o1}} \tag{6}$$

The device produced an efficiency of 35.8% with trap concentration fixed at $1 \times 10^{13}\,cm^{-3}$. Efficiency is constant up to a trap concentration value of $1 \times 10^{15}\,cm^{-3}$ and declined to 30.7% at $1 \times 10^{18}\,cm^{-3}$ trap concentration. Efficiency dropped by almost 4% beyond a trap concentration of $1 \times 10^{16}\,cm^{-3}$. Further simulations were carried out by fixing $1 \times 10^{16}\,cm^{-3}$ trap concentration value at top and bottom cells with MQW lifetime fixed at 16.7 ps. A comparison was carried out to study the radiation resistance of both the solar cells having MQW and p-i-n middle cells. For this, the base thickness and doping of both the cells were varied to

Table 3
Trap levels and capture cross section of InGaP, InGaAsN.

Material	Trap level (eV)	Type	Capture cross section σ(cm^2)
InGaP	Ec-0.36	acceptor	3×10^{-17} [37]
	Ec-0.72	acceptor	2.5×10^{-17} [37]
	Ev + 0.5	donor	4×10^{-16} [37]
	Ev + 0.76	donor	5×10^{-16} [37]
InGaAsN	Ec-0.2	acceptor	8.9×10^{-15} [11,38]

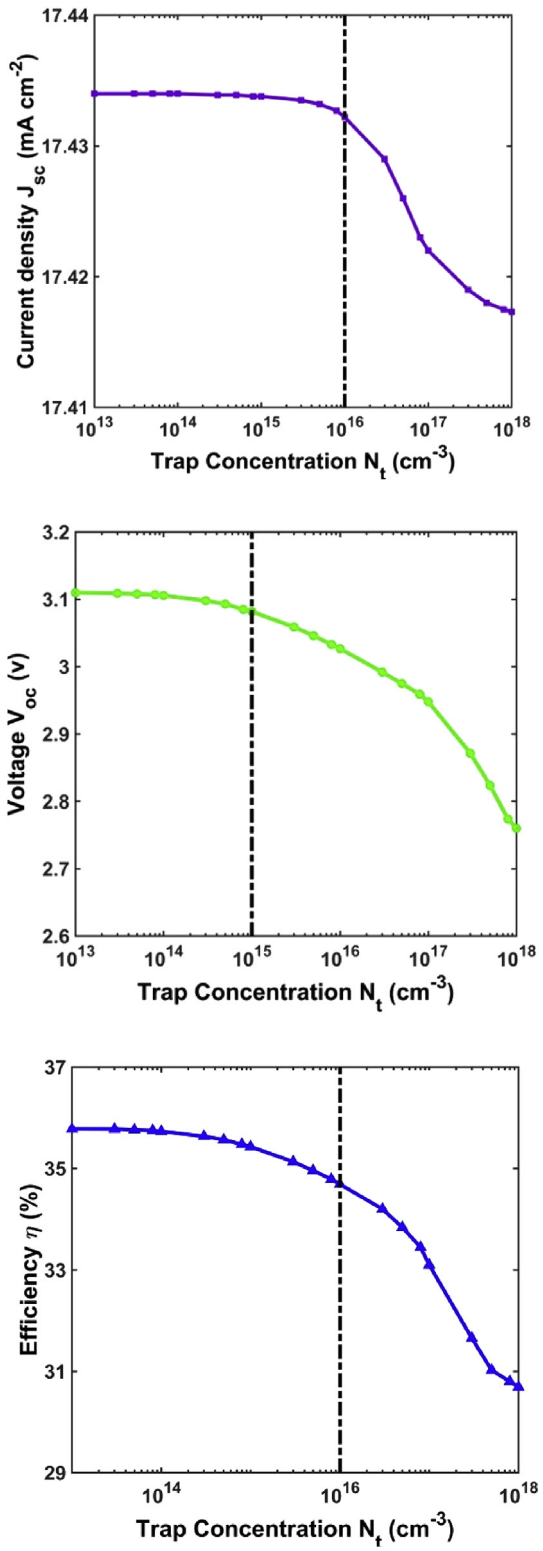

Fig. 4. 3J InGaP/InGaAs-GaAsP/InGaAsN solar cell output parameters (a) J_{sc} (b) V_{oc} (c) ηvariation as a function of trap concentration N_t, with traps introduced in top InGaP and bottom InGaAsN cells. MQW region background doping and lifetime were taken as n type-1 x 10^{16} cm^{-3} and 16.7 ps.

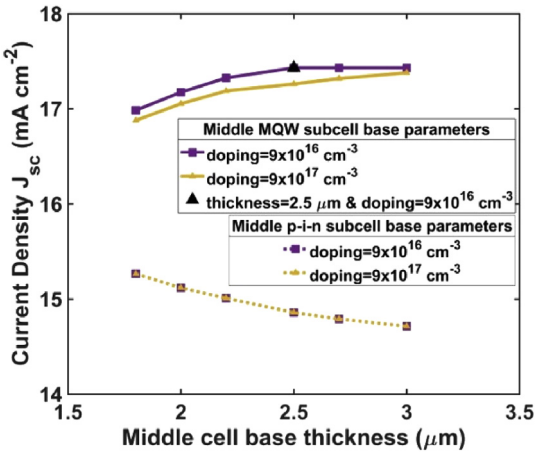

Fig. 5. Comparison of total cell J_{sc} as a function of middle MQW cell and middle p-i-n cell base thickness and doping at a fixed trap concentration of 1×10^{16} cm^{-3}. The lifetime and background doping of MQW region are 16.7 ps and 1×10^{16} cm^{-3} (n type) respectively.

generate total cell J_{sc} plot as shown in Fig. 5. 3J solar cell with middle MQW shows higher J_{sc} compared to 3J p-i-n solar cell. The middle cell base thickness and doping values considered in this paper are indicated in the same figure.

3.3. Power density of total and individual cells

The results under this section are generated by changing MQW region background doping from intrinsic to 1×10^{16} cm^{-3} (n-type), fixing the trap concentration of 1×10^{16} cm^{-3} for the trap levels defined in Table 3, and MQW region lifetime at 16.7 ps. Fig. 6 shows the power density plots as a function of solar cell bias voltage. The total cell produced a maximum power of 52 mW/cm^2 without defining traps in the material layers. We plotted the PV curves (dotted line) by fixing the trap concentration at 1×10^{16} cm^{-3} and the maximum power reduced by 8.5%. The percentage drop for top, middle, and bottom subcells are 8.3%, 12.2%, and 16.5% respectively. Individual subcell P-V curves with and without traps were presented in the same graph. Among the three subcells, the power density of the middle cell is 1.4 times the power achieved by the top cell and twice the power of the bottom cell. Clearly, all the three subcells experience power drop with traps affecting the minority carrier movement. The solar cell was simulated by increasing the number of suns, without introduction of traps to estimate the peak efficiency of the cell. The efficiency started at 38% for 1-sun and increased to 44% at 500 suns as shown in Fig. 7. We want to analyse the efficiency vs. sun concentration plot by fixing the trap concentration at 1×10^{16} cm^{-3} and SRV 1×10^4 cm s^{-1}. In this case, the efficiency reduced by around 3% compared to the former case. A maximum efficiency of 41.8% was achieved at 500 suns. The individual spectral response plots for 3J MQW multi-junction solar cell are presented in Fig. 8. The maximum quantum efficiency attained by the top, middle, and bottom subcells is 94%, 95%, and 80% respectively. EQE curve of middle p-i-n subcell without quantum wells is shown in the same figure. It can be noticed that the

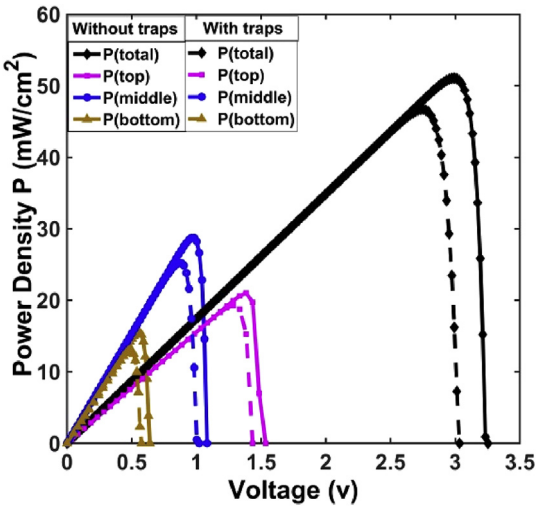

Fig. 6. Power density vs. bias voltage curves for total,top, middle, and bottom cells without defining traps and by defining traps in top and bottom cells. Middle MQW region lifetime was fixed at 16.7ps with a background doping of 1×10^{16} cm^{-3}-n type.

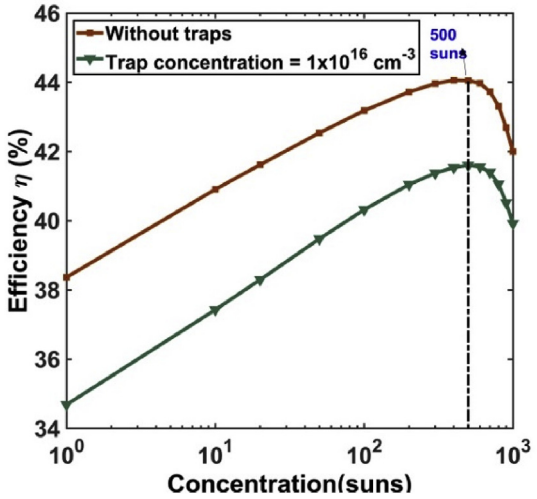

Fig. 7. Comparison of efficiency increment with increased sun concentration without defining traps and at $1 \times 10^{16}\,cm^{-3}$ trap concentration.

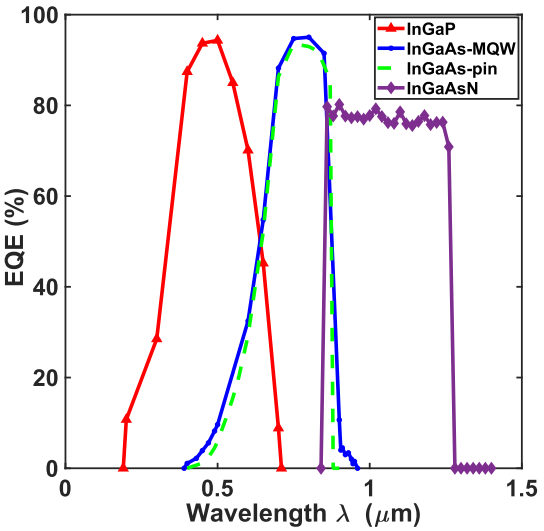

Fig. 8. EQE curves of 3J InGaP/InGaAs-GaAsP/InGaAsN solar cell. GaAs p-i-n cell EQE without quantum wells is shown as dotted line.

solar cell with middle MQW subcell has shown marginally higher EQE compared to the one without quantum wells. The photon absorption is increased in case of middle subcell with quantum wells which increases the EQE and hence the current density of the subcell. This statement can also be supported by Fig. 2. Also, for the solar cell with quantum wells, the absorption edge slightly extends at longer wavelengths inferring that more photons are absorbed at higher wavelengths leading to higher current density.

4. Conclusion

Incorporating InGaAs MQW in the middle cell intrinsic region and dilute nitrides at the bottom cell increases the efficiency compared to state-of-the-art InGaP/GaAs/Ge solar cell (31% 1 sun, AM0). The optimized structure produced an efficiency of 38% (1 sun, AM0 spectrum) which is 4% higher compared to 3J p-i- n GaAs solar cell and 7% higher compared to 3J p-n GaAs solar cell. The absorption edge of the middle cell can be engineered by the inclusion of quantum wells in InGaAs subcell. The influence of CR effect on electric field profiles across the MQW region was studied. The changed intrinsic region doping to n-type ($5 \times 10^{16}\,cm^{-3}$), due to CR effect, affects the uniformity of electric field intensity thereby influencing the carrier transport within the MQW region. Therefore, i-region doping should be less than ($1 \times 10^{16}\,cm^{-3}$) for maintaining uniform electric field strength. The paper also presents results on degradation of InGaP/InGaAs MQW/InGaAsN solar cell by considering irradiation induced deep level traps in the top and bottom subcells, while fixing the carrier lifetime of MQW region at 16.7 ps. The results infer that the percentage drop experienced by V_{oc} is high compared to J_{sc}, as the concentration of deep level traps increases. The onset of output parameter degradation can be observed from $1 \times 10^{16}\,cm^{-3}$ trap concentration. The device exhibited an efficiency of 34.6% at a trap concentration of $1 \times 10^{16}\,cm^{-3}$ fixed

for the top and bottom cells, with quantum well region lifetime and doping fixed at 16.7 ps and $1 \times 10^{16}\,cm^{-3}$ respectively. At increased sun concentration, the device attained maximum efficiency of 44% without traps and 42% with traps. It was shown that EQE of the middle cell with quantum wells attained marginally higher value compared to the one without MQW, along with increased absorption at longer wavelengths. From power density vs. bias voltage curves, it is the MQW middle cell that generates more power compared to the top and bottom cells individually. The enhanced performance and radiation tolerance of 3J MQW dilute nitride based solar cells make them potential devices to be incorporated in future for powering space satellites.

Acknowledgement

This work was supported by Indian Space Research Organisation under grant no ISRO/RES/3/719/16-17. The authors would like to thank UR Rao Satellite Center for providing the experimental data of InGaP/GaAs/Ge multi-junction solar cell.

Appendix A. Supplementary data

Supplementary data to this article can be found online at https://doi.org/10.1016/j.spmi.2019.04.009.

References

[1] C. Fetzer, R.R. King, D.C. Law, K.M. Edmondson, T. Isshiki, M. Haddad, X. Zhang, J.C. Boisvert, D.E. Joslin, N.H. Karam, Multijunction Solar Cell Development and Production Atspectrolab, (2007).
[2] H. Yoon, J.E. Granata, P. Hebert, R.R. King, C.M. Fetzer, P.C. Colter, K.M. Edmondson, D. Law, G.S. Kinsey, D.D. Krut, J.H. Ermer, Recent advances in high-efficiency III–V multijunction solar cells for space applications: ultra triple junction qualification, Prog. Photovolt. Res. Appl. 13 (2) (2005) 133–139.
[3] M. Meusel, C. Baur, G. L´etay, A. Bett, W. Warta, E. Fernandez, Spectral response measurements of monolithic GaInP/Ga(In) As/Ge triple-junction solar cells: measurement artifacts and their explanation, Prog. Photovolt. Res. Appl. 11 (8) (2003) 499–514.
[4] L. Zhang, P. Niu, Y. Li, M. Song, J. Zhang, P. Ning, P. Chen, Investigation on high-efficiency Ga0:51In0:49P/In0:01Ga0:99As/Ge triple-junction solar cells for space applications, AIP Adv. 7 (12) (2017) 125–217.
[5] H. Fujii, Y. Wang, K. Watanabe, M. Sugiyama, Y. Nakano, High-aspect-ratio structures for efficient light absorption and carrier transport in InGaAs/GaAsP multiple quantum well solar cells, 2012 IEEE 38th Photovoltaic Specialists Conference (PVSC) Part 2, IEEE, 2012, pp. 1–9.
[6] R. Kellenbenz, R. Hoheisel, P. Kailuweit, W. Guter, F. Dimroth, A.W. Bett, Development of radiation hard Ga0:50In0:50P/Ga0:99In0:01As/Ge space solar cells with multi quantum wells, Photovoltaic Specialists Conference (PVSC), 2010 35th IEEE, IEEE, 2010, pp. 000117–000122.
[7] N. Ashkenasy, M. Leibovitch, Y. Rosenwaks, Y. Shapira, K.W.J. Barnham, J. Nelson, J. Barnes, GaAs/AlGaAs single quantum well pin structures: a surface photovoltage study, J. Appl. Phys. 86 (12) (1999) 6902–6907.
[8] K.W.J. Barnham, G. Duggan, A new approach to high efficiency multi-band-gap solar cells, J. Appl. Phys. 67 (7) (1990) 3490–3493.
[9] K.W.J. Barnham, B. Braun, J. Nelson, M. Paxman, C. Button, J.S. Roberts, C.T. Foxon, Short-circuit current and energy efficiency enhancement in a low-dimensional structure photovoltaic device, Appl. Phys. Lett. 59 (1) (1991) 135–137.
[10] S.R. Kurtz, A.A. Allerman, E.D. Jones, J.M. Gee, J.J. Banas, B.E. Hammons, InGaAsN solar cells with 1.0 eV band gap, lattice matched to GaAs, Appl. Phys. Lett. 74 (5) (1999) 729–731.
[11] A. Khan, S.R. Kurtz, S. Prasad, S.W. Johnston, J. Gou, Correlation of nitrogen related traps in InGaAsN with solar cell properties, Appl. Phys. Lett. 90 (24) (2007) 243509.
[12] M.A. Green, K. Emery, Y. Hishikawa, W. Warta, E.D. Dunlop, Solar cell efficiency tables (version 41), Prog. Photovolt. Res. Appl. 21 (1) (2013) 1–11.
[13] M. Ochoa, I. Garc´ıa, I. Lombardero, L. Ayll´on, L. Cifuentes, I. Rey-Stolle, C. Algora, A.D. Johnson, J.I. Davies, K.H. Tan, W.K. Loke, Advances towards 4J lattice-matched including dilute nitride subcell for terrestrial and space applications, Photovoltaic Specialist Conference (PVSC), 2017 IEEE 44th, IEEE, 2017, pp. [1]–[6].
[14] R. Bestam, A. Aissat, J.P. Vilcot, High efficiency quadruple junction solar cells, Superlattice. Microst. 91 (2016) 22–30.
[15] D. Walker, J. Nocerino, Y. Yue, C.J. Mann, S.H. Liu, Subcell light current-voltage characterization of irradiated multijunction solar cell, E3S Web of Conferences, vol. 16, EDP Sciences, 2017, p. 02005.
[16] S. Park, Irradiation Effect in Triple Junction Solar Cells for Spatial Applications, PhD thesis Universit´e Paris-Saclay, 2018.
[17] P. Kailuweit, R. Kellenbenz, S.P. Philipps, W. Guter, A.W. Bett, F. Dimroth, Numerical simulation and modeling of GaAs quantum-well solar cells, J. Appl. Phys. 107 (6) (2010) 064317.
[18] S.R. Kurtz, D. Myers, J.M. Olson, Projected performance of three-and four-junction devices using GaAs and GaInP, Photovoltaic Specialists Conference, 1997., Conference Record of the Twenty-Sixth IEEE, IEEE, 1997, pp. 875–878.
[19] N.Y. Li, P.R. Sharps, J.S. Hills, H. Hou, P.C. Chang, A.G. Baca, Development of 1.25 eV InGaAsN for Triple Junction Solar Cells, Technical report, Sandia National Labs., Albuquerque, NM (US) Sandia National Labs., Livermore, CA (US), 2000.
[20] APSYS, 2016 Version by Crosslight, Software inc., Burnaby, Canada, 2016.
[21] S. Kotamraju, M. Sukeerthi, S.E. Puthanveettil, M. Sankaran, Study of degradation in InGaP/InGaAs/Ge multi-junction solar cell characteristics due to irradiation induced deep level traps using finite element analysis, Sol. Energy 178 (2019) 215–221.
[22] Z.Q. Li, Y.G. Xiao, Z.S. Li, Modeling of multi-junction solar cells by Crosslight APSYS, High and Low Concentration for Solar Electric Applications, vol. 6339, International Society for Optics and Photonics, 2006, p. 633909.
[23] Z.Q. Li, Y.G. Xiao, Z.S. Li, Two-dimensional simulation of GaInP/GaAs/Ge triple junction solar cell, Phys. Status Solidi C 4 (5) (2007) 1637–1640.
[24] G. Jiang Lin, J. Bi, M. Song, J. Liu, W. Xiong, M. Huang, III-V multi-junction solar cells, Optoelectronics – Advanced Materials and Devices, Chapter 18, InTech, Rijeka, 2013.
[25] S. Saylan, T. Milakovich, S.A. Hadi, A. Nayfeh, E.A. Fitzgerald, M.S. Dahlem, Multilayer antireflection coating design for GaAs0:69P0:31/Si dual-junction solar cells, Sol. Energy 122 (2015) 76–86.
[26] Y. Ö zen, N. Akın, B. Kınacı, S. Ö zc¸elik, Performance evaluation of a GaInP/GaAs solar cell structure with the integration of AlGaAs tunnel junction, Sol. Energy Mater. Sol. Cell. 137 (1–5) (2015).
[27] F.W. Ragay, J.H. Wolter, A. Marti, G.L. Araujo, Experimental Analysis of GaAs-InGaAs MQW Solar Cells vol. 2, (Dec 1994), pp. 1754–1758.
[28] K. Barnham, I. Ballard, J. Barnes, J. Connolly, P. Gri¸n, B. Kluftinger, J. Nelson, E. Tsui, A. Zachariou, Quantum well solar cells, Appl. Surf. Sci. 113 (1997) 722–733.
[29] C.I. Cabrera, J.C. Rimada, J.P. Connolly, L. Hernandez, Modelling of GaAsP/InGaAs/GaAs strain-balanced multiple quantum well solar cells, J. Appl. Phys. 113 (2) (2013) 024512.
[30] N.J. Ekins-Daukes, K. Kawaguchi, J. Zhang, Strain balanced criteria for multiple quantum well structures and its signature in X-ray rocking curves, Cryst. Growth Des. 2 (4) (2002) 287–292.
[31] C. Claeys, E. Simoen, Radiation Effects in Advanced Semiconductor Materials and Devices vol. 57, Springer Science & Business Media, 2013.
[32] M. Yamaguchi, C. Amano, Numerical analysis for radiation resistant GaAs heteroface solar cell structures, J. Appl. Phys. 57 (2) (1985) 537–544.

[33] S.M. Ramey, R. Khoie, Modeling of multiple-quantum-well solar cells including capture, escape, and recombination of photoexcited carriers in quantum wells, IEEE Trans. Electron. Devices 50 (5) (2003) 1179–1188.
[34] B. Van Zeghbroeck, Principles of Semiconductor Devices vol. 34, Colarado University, 2004.
[35] R. Hoheisel, M. Gonzalez, M.P. Lumb, D.A. Scheiman, S.R. Messenger, C.G. Bailey, J. Lorentzen, T.N.D. Tibbits, M. Imaizumi, T. Ohshima, S. Sato, Quantum-well solar cells for space: the impact of carrier removal on end-of-life device performance, IEEE J. Photovolt. 4 (1) (2014) 253–259.
[36] C. Besikci, M. Razeghi, Electron transport properties of Ga0:51/In0:49/P for device applications, IEEE Trans. Electron Devices 41 (6) (1994) 1066–1069.
[37] A. Khan, M. Yamaguchi, J.C. Bourgoin, T. Takamoto, Thermal annealing study of 1 MeV electron-irradiation-induced defects in n+ p InGaP diodes and solar cells, J. Appl. Phys. 91 (4) (2002) 2391–2397.
[38] A. Khan, J. Gou, S.R. Kurtz, S.W. Johnston, M. Imazumi, M. Yamaguchi, Dlts analysis of radiation-induced defects in InGaAsN solar cell structures, Photovoltaic Energy Conversion, Conference Record of the 2006 IEEE 4th World Conference on, vol. 2, IEEE, 2006, pp. 1858–1860.
[39] X. Wang, Z.M. Wang, High-efficiency solar cells.Physics, materials, and devices, Springer Mater. Sci. 190 (2014).
[40] M. Sukeerthi, S. Kotamraju, R. Meetei, P.N. Rao, Degradation analysis of 3J InGaP/InGaAs/InGaAsN solar cell due to irradiation induced defects with a comparative study on bottom homo and hetero InGaAsN subcell, Sol. Energy 174 (2018) 728–734.
[41] J. Nelson, M. Paxman, K.W.J. Barnham, J.S. Roberts, C. Button, Steady-state carrier escape from single quantum wells, IEEE J. Quantum Electron. 29 (6) (1993) 1460–1468.
[42] A.M. Fox, D.A. Miller, G. Livescu, J.E. Cunningham, W.Y. Jan, Quantum well carrier sweep out: relation to electro absorption and exciton saturation, IEEE J. Quantum Electron. 27 (10) (1991) 2281–2295.
[43] C.Z. Carlin, G.K. Bradshaw, J.P. Samberg, P.C. Colter, S.M. Bedair, Minority carrier transport and their lifetime in In-GaAs/GaAsP multiple quantum well structures, IEEE Trans. Electron. Devices 60 (8) (2013) 2532–2536.
[44] J.L. Gray, The physics of the solar cell, Handbook Photovolt. Sci. Eng. (2003) 61–112.